Microemulsion networks: the onset of bicontinuity

2000 J. Phys.: Condens. Matter 12 A253

(http://iopscience.iop.org/0953-8984/12/8A/332)

J. Phys.: Condens. Matter **12** (2000) A253–A262. Printed in the UK PII: S0953-8984(00)09283-3

Microemulsion networks: the onset of bicontinuity

T Tlusty and S A Safran

Department of Materials and Interfaces, The Weizmann Institute of Science, Rehovot 76100, Israel

Received 4 November 1999

Abstract. We predict theoretically the gradual formation of fluctuating, connected microemulsion networks from disconnected cylinders as the spontaneous curvature and the radius are varied, in agreement with recent direct measurements of these topological transitions. We discuss the role of the topological defects, the network junction and the end-cap of the disconnected cylinders, in the connectivity transition. The optimal shapes and curvature energies of the junctions and end-caps are calculated numerically and compared with analytic approximations.

1. Introduction

Microemulsions (ME), dispersions of polar (water) and non-polar (oil) fluids and amphiphile, exhibit an extremely rich variety of geometries. This behaviour is attributable to the amphiphilic molecules which reside at the interfaces between water and oil, thus reducing the bare water–oil tension by 3–5 orders of magnitude; this drastic reduction enables the formation of mesoscopic water and oil domains defined by amphiphilic interfaces which can assemble in many different shapes and sizes. Among these topologies, the multiply-connected *symmetric* sponge, in which the water and oil domains are both continuous, has been extensively studied [1]. These bicontinuous structures are observed around the inversion temperature, $\bar{T}$, where the preferred curvature of the amphiphilic monolayer towards water or oil (the spontaneous curvature) vanishes. Away from $\bar{T}$, this bicontinuity disappears and the amphiphilic monolayers were traditionally thought to form disconnected globules surrounded by a continuous domain of the other component.

Preliminary data from self-diffusion NMR and conductivity measurements [2,3] suggested the existence of bicontinuous structures even far from $\bar{T}$, where one would have expected a phase of disconnected globules [4]. Recently, we proposed a model for ME based on thermally fluctuating *asymmetric bicontinuous networks*, whose building blocks are cylinders interconnected by junctions [5]. Our model provides a direct link between the structural bicontinuity and the striking thermodynamic features that ME exhibit around $\bar{T}$: the generic, critical, re-entrant two-phase separation and the subsequent formation of a three-phase region [6] together with its remarkable ultra-low values of the three tensions at the interfaces [7] are all direct results of an entropic attraction induced by the network fluctuations. Moreover, the model explains the universal scaling properties observed in recent experimental studies by Strey and Sottmann, that show data collapse of both the phase diagrams [8] and tensions [9] of 19 different non-ionic ME systems. The latest, most conclusive evidence to support the network picture was provided by Bernheim-Grosswasser and Talmon who used cryogenic transmission

0953-8984/00/SA0253+10$30.00

electron microscopy (cryo-TEM) to directly observe the dilute, semi-flexible networks with their typical threefold 'Y-like' junctions [10], in both the single-phase and two-phase regions.

The fluctuating network model consistently predicts the topological transitions observed in ME when the spontaneous curvature, c_0, is decreased (in non-ionic ME, c_0 is controlled by the temperature as $c_0 \sim T - \bar{T}$): first, the ME evolves from spherical globules to long cylinders that subsequently interconnect via threefold junctions, leading to the formation of the bicontinuous network. The junctions interconnecting the cylindrical branches of the network are one type of topological defect of the infinite cylinders with a defect energy cost of the junction curvature energy, ϵ_3, relative to the cylinder bending energy. As usual, the defects are stabilized by the additional entropy that they afford the system since they increase the possible configurations of the ME network. We show below how this interplay between curvature energy and the network configurational entropy determines the network topology and the related free energy. Similarly, in ME composed of disconnected cylinders, the length distribution is determined by the balance between the curvature energy required to form the end-caps of the cylinders, ϵ_1, and their translational entropy. Moreover, we show that the *connectivity* transition when the network is formed from disconnected cylinders takes place when the junction and the end-cap energies are comparable, $\epsilon_3 \simeq \epsilon_1$ [11]. All this makes an accurate estimate of the curvature energies of these two types of topological defects a crucial ingredient of our theory, essential for understanding the relation between structure and thermodynamics and for comparison with experiment. In this paper, we briefly discuss the main concepts and results of the model, and present for the first time a calculation of the end-cap and junction curvature energies.

2. Network free energy and phase behaviour

Within the network, one can identify two length scales: the *local* length scale is the radius of the cylinders, R, that is governed by the curvature energy of the amphiphile interface. The *non-local, large-scale* length is the typical distance, L, between the network junctions, which is governed by the translational entropy of the junctions. Our theory traces the progression of the microstructure from the curvature-governed dilute network, $L \gg R \sim c_0^{-1}$, to the strong-fluctuation regime, where the junction defects proliferate, the typical distance between junctions becomes comparable with their size, $L \sim R \ll c_0^{-1}$, and they form a dense sponge.

As predicted by theory and confirmed by experiment [10], the bicontinuous ME network first appears at high spontaneous curvature, far from $\bar{T}$. In these regions, one can neglect the effect of short-wavelength thermal fluctuations and the *local* geometry of the ME is determined solely by the curvature energy of the amphiphile interface:

$$F_e = \frac{1}{2}\kappa \int \mathrm{d}S \left(\frac{1}{R_1} + \frac{1}{R_2} - 2c_0 \right)^2 + \bar{\kappa} \int \mathrm{d}S \left(\frac{1}{R_1} \frac{1}{R_2} \right) \tag{1}$$

where R_1 and R_2 are the principal radii of curvature, κ is the bending modulus and $\bar{\kappa}$ is the saddle-splay modulus. We discuss the sequence of transitions leading to the formation of the cylinders and then focus on their interconnection to form a bicontinuous network, a process governed by the entropy and the energetics of the junctions and the end-caps.

For bending constants, $\kappa \gg k_B T$, the curvature energy dominates and the free-energy density scales as $f_e = F_e/V = \phi r^{-3} E(r)$, where ϕ is the volume fraction of the inner phase (oil or water) and $r = c_0 R$ is the ratio of the radius to the optimal radius of curvature; $E(r)$ is the scale-invariant curvature energy. To find the stable local structure we compare the curvature energy of three possible geometries, spherical, cylindrical and lamellar. In a single phase the

radius is determined by the volume-to-surface ratio:

$$R = 2\delta \frac{\phi}{\phi_s} \tag{2}$$

where the volume fraction of the surfactant is ϕ_s and δ is the surfactant chain length (R is the cylinder radius, which is two-thirds of the sphere radius, and twice the inter-lamellar distance). The curvature energy of the cylinders is

$$E_c(r) = \kappa(1 - 4r) \tag{3}$$

while for spheres $E_s(r) = \frac{8}{9}(2\kappa(1 - 3r) + \bar{\kappa})$, where E_s and E_c are measured relative to the curvature energy of the lamellae $E_l = 0$. Comparing the curvature energies, one finds that the lamellae are optimal for $r < \frac{1}{4}$ (this region may be accessed by approaching the inversion temperature, $\bar{T}$, or alternatively by reducing the radius, R). As r increases there occurs a transition to cylinders, followed by a transition to a region where they coexist with spheres (around $r \simeq \frac{7}{12} + \frac{2}{3}\bar{\kappa}/\kappa$), and finally to a pure phase of spheres [4, 11].

The global structure of the cylindrical ME [4] is governed by entropy, due to the thermal fluctuations of its topological defects, the junctions and the end-caps [12]. To estimate the free energy, consider the network formed by an ensemble of cylinders of various lengths. The number density of cylinders of length m is $X(m)$, which obeys the volume conservation, $\int mX(m)\ \mathrm{d}m = \phi$. The branches are interconnected by z-fold junctions that each cost an energy ϵ_z (relative to the cylinders) due to their curvature. The number density of the junctions is z times smaller than the number density of free ends of the disconnected cylinders:

$$\rho_z = \frac{2}{z} \int X(m)\ \mathrm{d}m.$$

To obtain the free-energy density (in units of $k_B T$), one needs to take into account, apart from the translational entropy of the free cylinders (the first term of equation (4)), the curvature energy of the junctions (the second term) and the entropy (the last term) lost when each set of z free ends is constrained to form a junction [13]:

$$f_n = \int X(m)(\ln X(m) - 1)\ \mathrm{d}m + \rho_z \epsilon_z - (z - 1)\rho_z \ln \rho_z. \tag{4}$$

Minimizing the free energy (equation (4)) with respect to the length distribution $X(m)$, one finds that the junctions behave as an ideal gas of defects, in the sense that the entropy is $k_B T$ per junction, $f_n = -\rho_z$. The connectivity of the network together with the conservation laws for $X(m)$ imply that the number density of junctions, ρ_z, and the free energy scale as follows [13]:

$$f_n = -\rho_z \sim \phi^{z/2} \mathrm{e}^{-\epsilon_z}. \tag{5}$$

The $z = 1$ case corresponds to disconnected cylinders terminating at end-caps. The $z = 2$ 'junctions' may describe a one-dimensional system of defects along one infinite cylinder. These perturbations are taken into account by the thermal fluctuations of the cylinders, and become important only close to the cylinder $\leftrightarrow$ sphere transition, where the curvature energy of cylinders exceeds that of spheres. Connected networks are formed only for $z \geqslant 3$. Hereafter we consider only $z = 3$, Y-like junctions and $z = 1$ end-caps. In general, junctions of higher coordination number, $z > 3$, are also feasible, but occur very rarely [10]. This results from the $\phi^{z/2}$-scaling of the network free energy that favours low-z networks when the system is dilute, $\phi \ll 1$. High-genus junctions are also unfavourable due to the saddles introduced by their shape (topologically, each junction corresponds to $z/2 - 1$ handles). For the connected network ($z = 3$) the exponent ($\frac{3}{2}$) governing the dependence of the free energy on the volume fraction is higher than linear, resulting in an effective attraction. When the network is broken

into free cylinders ($z = 1$), the ideal gas of junctions is replaced by an ideal gas of end-caps, of number density ρ_1, that each cost curvature energy ϵ_1.

The network starts to form when the number of junctions exceeds the number of end-caps, at $\rho_1 \simeq \rho_3$. Comparing the topology-dependent part of the network free energy (equation (5)) for junctions and end-caps, we find that apart from a logarithmic correction, the network forms when the energies of the two defects are equal. The critical volume fraction for the cylinder-to-network transition is thus given by [11]

$$\epsilon_3 - \epsilon_1 \simeq \ln \phi. \tag{6}$$

The contribution of the Gaussian curvature, $K = 1/(R_1 R_2)$, to the elastic energy (equation (1)) is, by the Gauss–Bonnet theorem, a topological invariant determined solely by the total number of junctions and end-caps. The threefold junction and the end-cap have opposite topological contributions of $-4\pi\bar{\kappa}(z/2 - 1) = \pm 2\pi\bar{\kappa}$ [11]. The resulting $4\pi\bar{\kappa}$ difference between the curvature energies of the two defects may have implications for the ME structure and phase diagram, as discussed below.

3. Junction and end-cap shapes and energies

Apart from the difference in topology of the end-caps and junctions and the consequent saddle-splay energies, one needs to minimize the curvature energy due to the deviation of the mean curvature, $H = \frac{1}{2}(1/R_1 + 1/R_2)$, from its preferred value, the spontaneous curvature, $2\kappa \int (H - c_0)^2 \, \mathrm{d}S$. The construction of a defect requires amphiphilic molecules and an inner phase which need to be taken from the cylinders. This is taken into account by considering the cylinders as a large reservoir coupled to the defects by its chemical potentials (surface tension and osmotic pressure):

$$\epsilon_z = F_z - \left(\frac{\partial F_c}{\partial S}\right)_V S_z - \left(\frac{\partial F_c}{\partial V}\right)_S V_z \tag{7}$$

where F_z is the curvature energy of the defect (equation (1) for a junction or end-cap), V_z its volume and S_z its surface area; the chemical potentials are derivatives of the cylinder curvature energy, $F_c = \phi r^{-3} E_c(r) V$ with respect to change in their surface and volume. Substituting the cylinder curvature energy E_c (equation (3)) in the potentials of equation (7) results in a scale-invariant defect energy:

$$\epsilon_z = 2\kappa \int \mathrm{d}s_z \, (h^2 - 2rh) - \kappa\left(\frac{3}{2} - 4r\right)s_z - \kappa(4r - 2)v_z \tag{8}$$

where $r = c_0 R$, $h = HR$, $s_z = S_z R^{-2}$ and $v_z = V_z R^{-3}$ are the normalized spontaneous curvature, mean curvature, surface area and volume, respectively. The effective osmotic pressure, $\Pi = \kappa(2 - 4r)$, becomes negative for $r > \frac{1}{2}$. This manifests the instability of the cylinders to emulsification failure—that is, the rejection of the excess internal phase to optimize the curvature energy [14]. Functional minimization of equation (8) yields cumbersome Euler–Lagrange equations which were numerically solved only for the simplified case of axial symmetry [15]. Below, we describe the results of a direct numerical minimization using the optimization code SURFACE EVOLVER [16] and compare them to those obtained by a simplified single-parameter variation approach, which provides some physical insight into the exact results of the simulation. The structures of both junction and end-cap were confirmed in recent measurements by Bernheim-Grosswasser and Talmon [10, 11].

Two typical, numerically optimized junctions are depicted in figure 1. The amphiphile interface is represented by an open triangulated grid of points which evolve under the influence

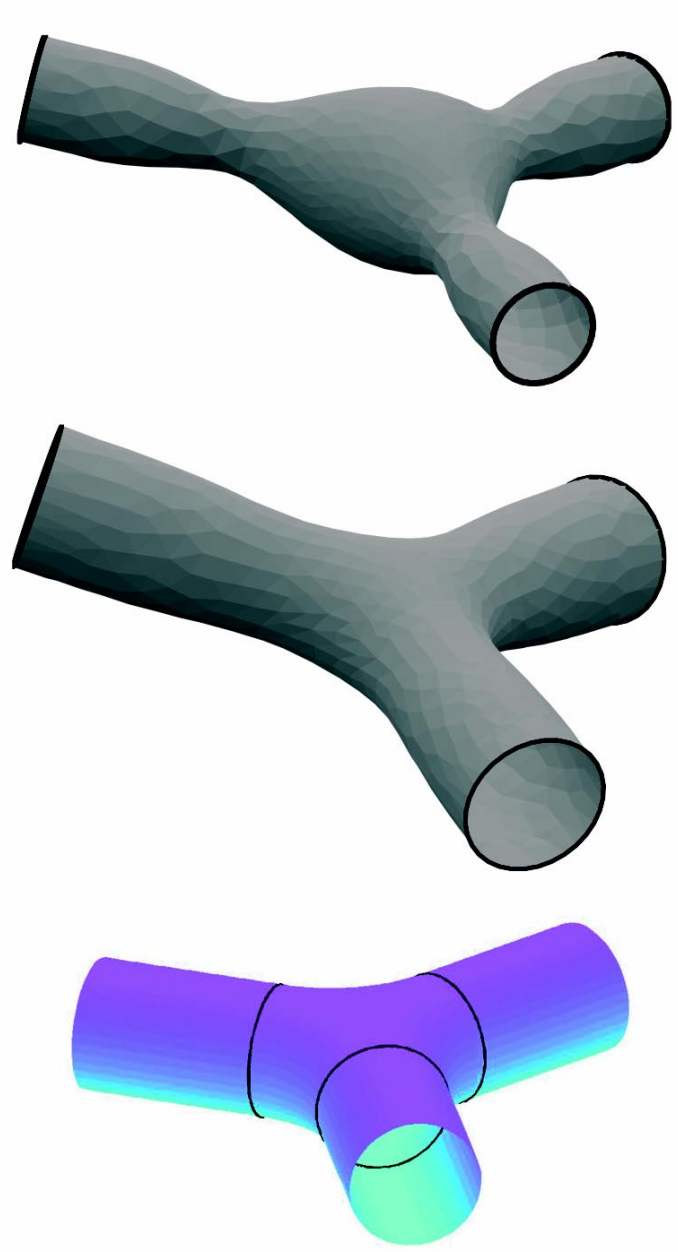

Figure 1. *The optimal shape of the threefold 'Y-like' junction.* Numerical optimization at high curvatures, $r = c_0 R = 0.5$, shows that the junction develops an enlarged spherical core with necks connecting to the cylinders (top). At smaller spontaneous curvatures, $r = c_0 R = 0.3$, we find that the junction develops a lamellar core, reflecting the fact that the system approaches the region where flat lamellae are the preferred local geometry (middle). This shape is similar to the analytic approximation (bottom), a lamellar core smoothly attached to three semi-toroidal segments. Each semi-toroidal segment is a sixth of the inner part of the torus. The smooth connections to the cylinders are denoted by dark rings.

of pseudo-forces derived from the energy integral (equation (8)) [16]. The boundary conditions are smooth connections of the minimized junction interface to three coplanar cylinders of radius $R = 1$ (since the problem is scale invariant) meeting at angles of $\frac{2}{3}\pi$. Observing the progression of the shape of the junction as the spontaneous curvature is changed, we find two regimes. At small spontaneous curvatures, $r = c_0 R < 0.3$, we find that the junction develops a lamellar core, reflecting the fact that the system approaches the region where flat lamellae are the preferred local geometry. At higher curvatures, $0.3 \leqslant r < 0.5$, we approach the region of spherical local geometry and the junction develops a spherical core with necks connecting to the cylinders. When we further increase the curvature, to $r > 0.5$, we find that the junction is unstable with respect to emulsification failure. In simulation, this instability is manifested by the 'explosion' of the core. The numerical minimization yields an approximately linear scaling of the junction energy with the spontaneous curvature (figure 2):

$$\epsilon_3 \simeq 4\pi\kappa(\alpha_3 r + \beta_3) \tag{9}$$

with $\alpha_3 \simeq 1.3$ and $\beta_3 \simeq -0.5$. We note that the ϵ_3 becomes negative for $r < -\beta_3/\alpha_3 \simeq 0.38$, even before the stable local geometry becomes lamellar. In simulation, junctions in this region tend to split into three junctions by puncturing the middle core. However, these negative-energy junctions may still be stabilized by three additional effects:

(i) For small enough saddle-splay modulus, $\bar{\kappa}$, the topological 'charge' of the junction, $-2\pi\bar{\kappa}$, may overcome the negative ϵ_3.

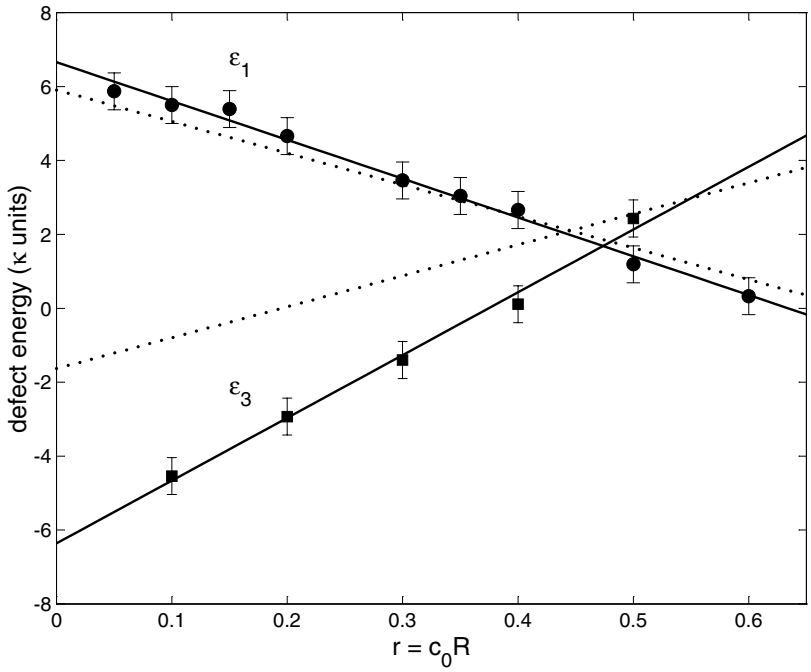

Figure 2. *Curvature energy of the defects.* Numerical optimizations of the curvature energy of junctions (ϵ_3—solid squares) and end-caps (ϵ_1—solid circles) exhibit an approximately linear scaling in $r = c_0 R$ (linear fits—solid lines). Junctions are optimal for small values of the normalized spontaneous curvature, r, due to their flat lamellar core, while end-caps are preferred at larger r because of their spherical cap. The numerical results are compared to the analytic approximations (dotted lines).

(ii) When the junctions proliferate they repel each other due to the curvature energy cost of the finite-length cylinders whose shape and energies have been modified by the nearby junctions.

(iii) As we discuss below, when the radius of the cylinders becomes comparable with the thickness of the amphiphile interface, one should introduce higher-order terms into the curvature energy.

An analytical approximation to the junction interface is depicted in figure 1: the junction is constructed from a lamellar core smoothly attached to three semi-toroidal segments of inner radius $R = 1$ and outer radius R_T, which is the parameter to be optimized. Each semi-toroidal segment is a sixth of the inner part of the torus. Integrating equation (8) over the surface of the junction we obtain

$$\epsilon_3 = \pi\kappa\left(\frac{2\tau^2}{\sqrt{\tau^2-1}}\arctan\sqrt{\frac{\tau+1}{\tau-1}} + \left(\frac{\sqrt{3}}{\pi} - \frac{1}{2}\right)\tau^2 - \frac{1}{2}\pi\tau + \frac{1}{3}(8r-7)\right)$$

where $\tau = R_T/R$ is the ratio of the outer and inner radii of the torus. Minimizing the latter expression, we find that optimal outer radius, and thus the junction shape, is independent of c_0, with $\tau = R_T/R \simeq 2.59$. The resulting junction energy is $\epsilon_3 \simeq 4\pi\kappa(\frac{2}{3}r - 0.13)$. This analytical approximation (figure 2) exhibits the same qualitative behaviour as the numerical solution of equation (9). The energy reflects the interplay between the tendency to enlarge the preferred lamellar core and the need to keep the outer radius of the torus small enough to compensate by its negative curvature, $0 \geqslant 1/R_1 \geqslant -1/R_T$, the positive curvature of the circular cross section, $1/R_2 = 1/R$. However, the approximation strongly deviates from the numerical solution for small r, mainly because the lamellar core cannot adjust its thickness, which is constrained to be equal to the diameter of cylinders. One may improve the poor agreement with simulation by relaxing this constraint, adding the ratio of core and cylinder widths as a second variational parameter [12].

The optimized shape of the end-cap, ϵ_1, exhibits an opposite dependence on the parameter $r = c_0R$ (figure 2): due to their enlarged spherical cap (figure 3) the end-caps cost more curvature energy at small r, where the preferred geometry is lamellar. The numerical minimization yields

$$\epsilon_1 \simeq 4\pi\kappa(\alpha_1 r + \beta_1) \tag{10}$$

with $\alpha_1 \simeq -0.84$ and $\beta_1 \simeq 0.54$. To obtain an analytical approximation we describe the end-cap as composed of two parts: a semi-spherical cap smoothly connected to the cylinder by a constant-mean-curvature, trumpet-like interface (figure 3). The axially symmetric interface is described by the profile of the radius $y(z)$ determined by the constant-mean-curvature constraint [15]:

$$\sin\theta = (1 + (\partial_z y)^2)^{-1/2} = (y + R_s R/y)/(R + R_s)$$

where R_s is the radius of the spherical cap to be optimized; the principal curvatures are $1/R_1 = \sin\theta/y$ and $1/R_2 = d_y \sin\theta$. The resulting curvature integral (equation (8)) is

$$\epsilon_1 = \frac{1}{3}\pi\kappa\left[\mu\left(\frac{\mu}{\mu+1}(4\mu^2+\mu-8) - 4[\mu(2\mu-3)+2]r + 7\right)E\left(\sqrt{1-\mu^{-2}}\right)\right.$$
$$\left. + \left(\mu(4\mu-9) - 8[(\mu-3)\mu+3]r\right) + 2\mu(2r-1)K\left(\sqrt{1-\mu^{-2}}\right) + 12\right]$$

where $\mu = R_s/R$ is the ratio of the sphere and cylinder radii. Optimizing the radius of the spherical cap, we obtain from the latter expression $\epsilon_1 = 4\pi\kappa(-0.68r + 0.47)$, in good agreement with the numerical solution (equation (10)), as depicted in figure 2. Here, the small

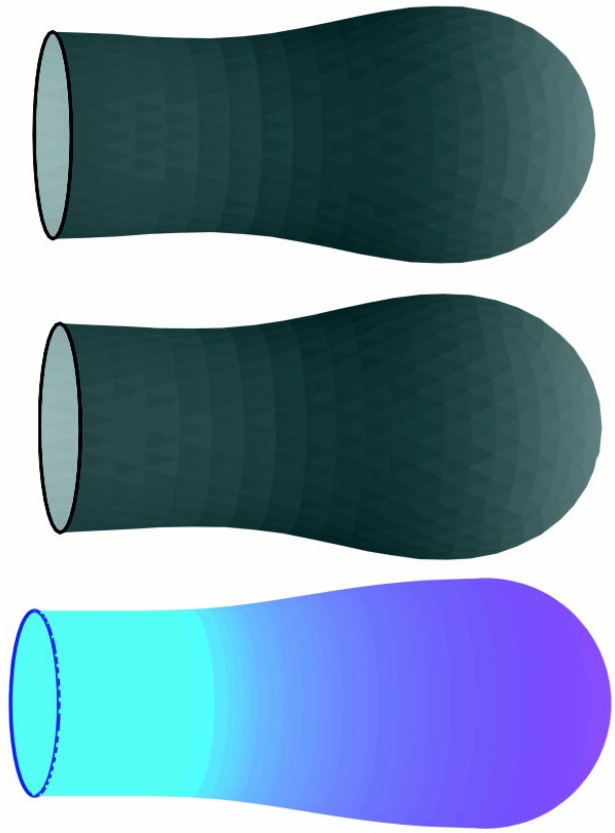

Figure 3. *The optimal shape of the end-cap.* The typical enlarged spherical cap is smoothly connected to the cylinder by a trumpet-like interface (these connections are denoted by dark rings). The numerical optimization shows no significant difference between the shapes of the optimal end-caps at high curvature (top—$r = c_0 R = 0.5$) and low curvature (middle—$r = 0.2$). The analytic, constant-mean-curvature approximation yields a similar shape (bottom).

deviations occur mainly because of a neck between the 'trumpet' and the cylinder that develops in simulation in the small-r region (figure 3).

The difference in elastic energy of the junction and end-cap, as calculated by the numerical or variational minimization described above, scales approximately linearly with r:

$$\epsilon_3 - \epsilon_1 = 4\pi\kappa((\alpha_3 - \alpha_1)r + (\beta_3 - \beta_1)) - 4\pi\bar{\kappa}$$

where the last term accounts for the opposite topological 'charge'. Junctions are optimal for small values of the normalized spontaneous curvature due to their flat lamellar core, while end-caps are preferred at larger r because of their spherical cap (figures 1–3). Substituting in equation (6) produces an expression for the value of $r = c_0 R$ at the cylinders-to-network transition at $r = r_n$ with [11]

$$r_n = \frac{1}{\alpha_3 - \alpha_1}\left((\beta_1 - \beta_3) + \frac{\bar{\kappa}}{\kappa} + \frac{1}{4\pi\kappa}\ln\phi\right). \tag{11}$$

The theoretical prediction described above, for the series of topological transitions leading to the formation of a network, spheres $\rightarrow$ spheres + cylinders $\rightarrow$ cylinders $\rightarrow$ network, was

recently substantiated by direct cryo-TEM measurements on non-ionic ME [10].

To accurately describe the elastic energy of ME systems with relatively small radii of curvature $R \sim \delta$, and especially to approach the limit of binary micellar ME (with no internal phase), one needs to take into account the details of the molecular interactions [12]. Here we approximate these effects by adding to the harmonic bending energy the next-order term, of third order in the principal curvatures. Expanding the elastic energy (equation (1)) for curvatures at a parallel surface, we find that the third-order term is proportional to $\kappa\delta(c_0 - H)(H^2 + c_0 H - K)$. We consider only the surface integral over H^3 and HK, since all other third-order terms contain powers of c_0 and therefore vanish in the binary limit, $r = c_0 R = 0$; for large values of r these terms are negligible compared to the harmonic bending energy. Using our results for the typical shapes of the end-cap and junctions, we find that this contribution, $2\kappa\delta \int \mathrm{d}S\ (KH - H^3)$, is negative for the end-cap and positive for the junction and scales as

$$\bar{\epsilon}_z = \gamma_z \kappa \frac{\delta}{R} = \gamma_z \kappa \frac{c_0 \delta}{r} \tag{12}$$

with $\gamma_1 < 0$ and $\gamma_3 > 0$, both of order unity. The third-order term, $\bar{\epsilon}_z$, inverts the behaviour of ϵ_z close to the binary limit, $r = 0$ (the actual radius at the binary limit is the molecular length, $r \simeq c_0\delta$). We therefore find a maximum in ϵ_1 and a minimum of ϵ_3 at typical radii which scale like $R_* \sim (\delta/c_0)^{1/2}$ (or $r_* \sim (c_0\delta)^{1/2}$).

The minimum in ϵ_3 has important implications for the ME phase diagram. The bicontinuous network exhibits a unique instability which directly results from its global connectivity: the entropic part of the free energy is unstable to phase separation when the effective attraction, $f_n = -\rho_z \sim -\phi^{z/2}\mathrm{e}^{-\epsilon}$, overcomes the repulsion. This occurs for values of the junction energy lower than a critical value. Since $\phi^{z/2}$ represents an effective attraction only if the exponent is higher than linear (or $z \geqslant 3$), we find that this type of phase separation is unique for the connected structures. The curvature energy of the junction exhibits a minimal value at r_* which corresponds to a steep maximum of the attraction due to its exponential dependence $\sim\mathrm{e}^{-\epsilon_3}$. When the maximal attraction exceeds the critical value, the ME phase separates into two networks of the same local geometry, cylindrical of radius r, which differ in the density of junctions, as verified by experiment [10]. This explains the re-entrant phase separation loops and the subsequent three-phase coexistence, which emerge as direct results of the non-monotonic behaviour of the junction energy, $\epsilon_3(r)$ [5]. In the phase diagram this *global* instability is manifested by the appearance of a two-phase coexistence loop bounded by two critical points.

Acknowledgments

The authors thank R Strey, T Sottmann, A Bernheim Grosswasser and Y Talmon for fruitful collaboration and inspiring discussions. We thank K Brakke and U S Schwarz for their help in using SURFACE EVOLVER, the numerical minimization software. We are grateful to the Research Centre on Self-Assembly of the Israel Science Foundation and the Minerva Gerhard Schmidt Centre for Supramolecular Architecture.

References

[1] Gelbart W M, Ben-Shaul A and Roux D (ed) 1994 *Micelles, Membranes and Microemulsions and Monolayers* (Berlin: Springer)
[2] Strey R, unpublished
[3] Lipgens S, Schūbel D, Schlicht L, Spilgies J H, Ilgenfritz G, Eastoe J and Heeman R K 1998 *Langmuir* **14** 1041

[4] Safran S A, Turkevich L A and Pincus P A 1984 *J. Physique Lett.* **45** L19
[5] Tlusty T, Menes R, Safran S A and Strey R 1997 *Phys. Rev. Lett.* **78** 2616
[6] Kahlweit M, Strey R and Busse G 1990 *J. Phys. Chem.* **94** 3881
[7] Aratono M and Kahlweit M 1991 *J. Chem. Phys.* **95** 8578
Kahlweit M, Strey R and Busse G 1993 *Phys. Rev.* E **47** 4197
[8] Sottmann T and Strey R 1997 *J. Chem. Phys.* **106** 8606
[9] Sottmann T and Strey R 1996 *J. Phys.: Condens. Matter* **8** A39
[10] Grosswasser A B, Tlusty T, Safran S A and Talmon Y 1999 *Langmuir* **15** 5448
[11] Tlusty T, Safran S A and Strey R 2000 *Phys. Rev. Lett.* **84** 1244
[12] May S, Bohbot Y and Ben-Shaul A 1997 *J. Phys. Chem.* B **101** 8649
[13] This mean-field approach was applied to micellar solutions:
Drye T J and Cates M E 1992 *J. Chem. Phys.* **96** 1367
and for a spin $n \to 0$ approach see
Elleuch K, Lequeux F and Pfeuty P 1995 *J. Physique* I **5** 465
[14] Safran S A and Turkevich L A 1983 *Phys. Rev. Lett.* **50** 1930
Leaver M S and Olsson U 1994 *Langmuir* **10** 3449
[15] Deuling H J and Helfrich W 1976 *J. Physique* **37** 1335
[16] K Brakke's Manual and Code for SURFACE EVOLVER may be downloaded at
http://www.susqu.edu/facstaff/b/brakke/evolver/evolver.html
http://www.geom.umn.edu/software/download/evolver.html